

## **SUPPLEMENTAL METHODS**

### **Creation of chronic MI**

After pericardial access, an anteroapical MI was created by microbead occlusion of the left anterior descending (LAD) artery at the 2<sup>nd</sup> diagonal branch as previously described(2,32,33). Briefly, through an AL-2 or Mach-1 catheter (8Fr, Amplatz-type catheter, Boston Scientific) under fluoroscopy, a luminal angioplasty balloon (3mm, Abbott Vascular, Armada™35) was advanced using an over-the-wire (0.014” Hi-Torque Balance Middleweight Universal, Abbott Vascular) technique. The balloon was then inflated at the 2<sup>nd</sup> diagonal branch of LAD artery, and 3.5mL of polystyrene – microspheres (90  $\mu$ m diameter, Polyscience Inc., Washington, PA, USA) was injected. ST-segment elevation, hyperacute T waves, and/or inverted T waves were noted on the surface ECG. A left ventriculogram confirm anteroapical wall motion abnormalities. Subjects were then extubated after weaning sedation, and then monitored carefully.

### **Terminal Experiment**

Terminal studies were performed 4-5 weeks following sham, MI, or MI+RTX intervention. Sedation and, intubation were performed as described above. Echocardiographic assessment was performed after sedation and while the heart was closed. Arterial blood pressure was monitored continuously from the left femoral artery using a pressure catheter (SPR350, Millar Inc, Houston, TX, USA). ECGs were also continuously recorded during the experimental protocol, and arterial blood gas was evaluated hourly. Fentanyl citrate (20  $\mu$ g/kg) was administered intravenously prior to sternotomy. The pericardium was opened in order to expose the heart, as well as both

stellate ganglia. Following completion of surgical procedures, isoflurane was gradually tapered off and switched to  $\alpha$ -chloralose (6.25mg/125mL; 1mL/kg for bolus, 20-35mL/kg or titrated to effect for maintenance) for in - vivo neural recordings from the left stellate ganglion. The left carotid artery was exposed, and a pressure catheter (SPR350, Millar Inc, Houston, TX, USA) was inserted in order to continuously monitor left ventricular pressure. Both the right and left vagus nerves were also exposed for bilateral vagal nerve stimulation (BVNS). Subjects were kept covered and heated using water blankets (37-38 °C), and a saline drip (8-10ml/kg/hour) was continuously given intravenously. At the end of the study, subjects were euthanized under deep sedation of isoflurane and cardiac fibrillation was induced.

## **Terminal study protocol**

### **Cardiac stressors**

After the experimental preparation described above, a twenty-minute waiting period was allowed for stabilization. Various stressors (right stellate ganglia stimulation, BVNS, inferior vena cava (IVC) occlusion, aortic occlusion, and right ventricular endocardial pacing) were performed in a random order. For the right stellate ganglia stimulation (RSGS), bipolar electrodes were inserted into right stellate ganglia. Repeated square-wave pulses at a 4, 8, and 10Hz frequency, 4ms pulse width, and at 2x threshold were introduced for 30 seconds using a Grass S88 Stimulator (Grass, Warwick, RI). The threshold was determined at a 10% increase in heart rate and/or blood pressure. BVNS was achieved using bipolar spiral cuff electrodes (Cyberonics) that were deployed around the vagus nerve bilaterally. Threshold was determined as a 10% decrease in

heart rate and the stimulation was performed at 2 times the threshold value (MI-RVNS:  $4.68 \pm 0.57$  mA, MI-LVNS:  $5.6 \pm 2.36$  mA, MI+RTX-RVNS:  $4.75 \pm 1.11$  mA, MI+RTX-LVNS:  $3.90 \pm 0.82$  mA) with a frequency/pulse width of 10Hz/1ms, 15Hz/1ms and 20Hz/1ms, each for 30 seconds. Decremental right ventricular pacing (RVP) was performed with a cycle length(CL) of 450ms (133 beats/minute) to 250ms (240 beats/minute) down by 50ms steps over 100 seconds using the Micropace (EP320) and Prucka CardioLab System (GE Healthcare). Bradykinin and Capsaicin (20 $\mu$ g/mL) applied epicardially to the ventricles were used to activate TRPV1 afferents. The heart was washed with warm saline 10 minutes after application and a 30-minute waiting period was allowed for recovery of the baseline hemodynamic function.

### **Tolerance for malignant arrhythmias**

Arrhythmia tolerance was tested using cesium chloride (84mg/kg) and programmed electrical stimulation (PES). Cesium chloride was injected intravenously via the femoral vein, and then flushed with 1mL warm saline. The reaction was assessed for 10 minutes and the experiment was continued only once the heart rate reached baseline levels. PES was performed using 8 beats of stimulus drive train (S1), followed by an S2 extrastimulus with a 10ms decrement down to a CL of 200ms (300 beats/minute) or effective refractory period (ERP). CL (S1) was determined as within 10% below the baseline CL. The beginning of the next extrastimulus (S2, S3, S4, S5) was defined at 75% of S1 CL. If the extrastimulus (S2) reached ERP without showing sustained ventricular tachycardia or ventricular fibrillation, the next extrastimulus (S3, up to S4,

S5) was then added. PES was performed using the Micropace (EP320) and Pruca CardioLab System (GE Healthcare).

### **Cardiac mapping for Activation Recovery Interval**

A 64- or 128-electrode array (2mm inter-electrode spacing, Neuronexus, Ann Arbor, MI) was placed on the left anterior epicardium in order to map cardiac electrical signals. Activation recovery interval (ARI), a surrogate marker of action potential duration (APD)(33,34), was obtained from the difference between recovery times (RT) and activation times (AT) using the customized software ScalDyn M (University of Utah, Salt Lake City, UT). RT was measured from the beginning of the QRS complex to the first maximum  $dV/dt$  of the T wave. AT was measured from the beginning of the QRS complex to the first minimum  $dV/dt$  in the QRS complex. Electrical maps of AT and ARI distributions were plotted using Map3D software (Center for Biocomputing, University of Utah, Salt Lake City, UT).

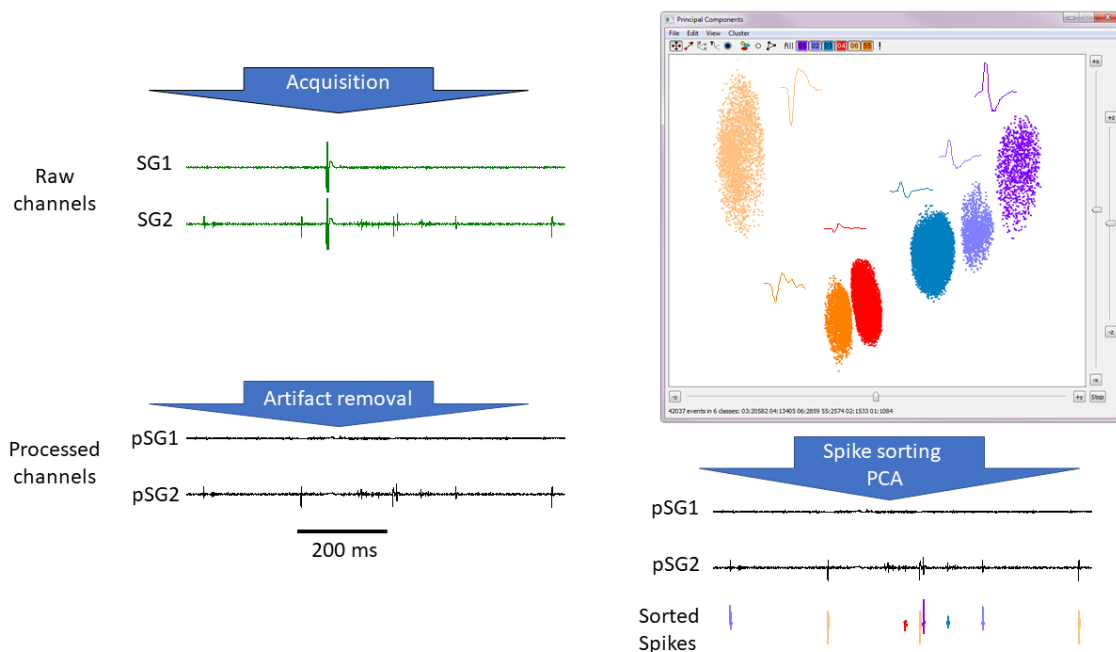
### **Stellate ganglion extracellular neuronal recordings**

A linear microelectrode array (LMA, 16 channels, Microprobes, Gaithersburg, MD) was inserted into the craniomedial pole of the left stellate ganglion. The platinum-iridium electrodes consisted of  $25\mu\text{m}$  surface area,  $500\mu\text{m}$  interelectrode spacing and 0.2-0.5 M $\Omega$  impedance. A microelectrode amplifier (Model 3600, A-M Systems Inc., Carlsborg, WA, USA) was used to acquire amplified signals. These electrode characteristics enable recordings of soma action potentials, not axons of passage in the stellate ganglion. Neuronal recording signals were filtered at 300Hz to 3kHz, with a gain of

1000-2500 and transferred into a data acquisition platform (Power1401, Cambridge Electronic Design, Cambridge, UK). Artifacts were identified and removed by recognizing similar and simultaneous waveforms on all 16 channels. Neuronal spikes were sorted using Spike2 software (Cambridge Electronic Design) and further neural analysis was done using Matlab (Matlab 2017b, The MathWorks, Inc., Natick, MA, USA) as previously described(1,2,14).

The approach taken for spike sorting utilized a widely available software package (Spike2™, Cambridge Electrical Design (CED), Cambridge U.K.). Using Spike2™, multi-unit neural recordings (such as that in this study) were processed for artifact removal, following which a 2:1 signal to noise ratio was set as the threshold for signals processed was set. Neural events (neuronal action potential spikes) are marked by crossing this threshold. All captured spikes are then processed using a combination of “template matching” and “cluster cutting” based on principal component analysis (PCA)(35). Measurements correlation analysis (based on morphology of the neuronal AP e.g. AP amplitude, positive or negative deflections, number of deflections, etc (parameters examined in the PCA) as shown in the figure below) is then used to sort spikes into different units based on templates

Finally, the data are subjected to cluster cutting methods to plot the spikes into a 3D view that can be rotated to confirm clear separation of the clusters of spikes. Clusters are determined by automatic algorithms, and further manual clustering is performed to separate or regroup clusters if needed. An abbreviated workflow is shown below. In this image, an example of two adjacent channels, SG1 and SG2 is shown. SG1 has no signals while SG2 does. The common signal in both channels is an artifact (present on



all channels in the array). This is filtered out. After the analyses described above, the 6 unique spikes that compose the entire channel and their morphologies are shown in the window (top right) panel. This is a 3D window that is shown in 2D here, however, the window can be rotated in 3D to ensure the clusters of neurons are separate. The panel on the bottom right part of the image shows the individual neuronal shapes and their associated inscriptions on channel SG2.

## **Tissue collection, Processing, and Immunohistochemistry**

The left ventricular myocardium (scar / border zone / remote), right stellate ganglia, and dorsal root ganglia were collected for immunohistochemistry. Tissues were rapidly collected post mortem, rinsed in cooled 0.1M phosphate buffered saline (PBS), and fixed in 4% paraformaldehyde (15714, Electron Microscopy Sciences, Hatfield, PA, USA) for 24 hours at 4 °C. Fixed tissues were washed with PBS for 4 times every 30minutes and then preserved in PBS with 0.1% sodium azide. Each fixed tissue was embedded in 2% agarose-PBS and was sliced in 200µm-thick sections for immunostaining using a microtome (VT 1200S, Leica Biosystems Inc., Buffalo Grove, IL, USA). Sliced segments were placed in 4% horse serum (ab7484, Abcam, Cambridge, MA, USA) prior to antibody staining (primary for 3 days, secondary for 2 days; listed in table below) in PBS with 0.1% Triton X-100 (X100, Sigma-Aldrich, St. Louis, MO, USA) at room temperature. A Zeiss LSM 780 confocal microscope (Carl Zeiss Oberkochen, DE) was used for imaging. Laser power and gain remained constant across all samples in order to facilitate comparison. Analytic software Zen (Black edition, Carl Zeiss Microimaging, Jena, DE) was used for digital image storage and was then evaluated and quantified using Image J (a public domain, java-based program developed at the U.S. National Institute of Health <https://imagej.nih.gov/ij/>).

For connexin43, the left ventricular myocardium was cut along the midline from the epicardial to the endocardial end, and then paraffin-embedded sections were cut at a thickness of 4µm. The paraffin was removed with xylene and rehydrated through graded ethanol. Endogenous peroxidase activity was blocked with 3% hydrogen peroxide in

methanol for 10minutes. Heat-induced antigen retrieval (HIER) was carried out for all sections in 0.01M citrate buffer (pH=6.00) using a Biocare decloaker at 95 °C for 25 minutes. The slides were then incubated for 1hour at room temperature with rabbit polyclonal Cx43 at 1/1000 dilution. The signal was detected using the Dakocytomation Envision A System Labelled Polymer HRP anti-rabbit (Agilent, K4003) and visualized with the diaminobenzidine reaction. The slides were counterstained with hematoxylin, dehydrated and coverslip.

List of antibodies used.

<b>Primary Antibody</b>	<b>Concentration</b>	<b>Source</b>
Protein Gene Product 9.5	1:500	Polyclonal Rabbit Antibody. Abcam. San Francisco, CA. ab108986.
Tyrosine Hydroxylase	1:200	Polyclonal Sheep Antibody. EMD Millipore. Darmstadt, Germany. ab1542.
Calcitonin Gene-Related Peptide	1:500	Monoclonal Mouse Antibody. Abcam. San Francisco, CA. ab81887.
Connexin 43	1:1000	Polyclonal Rabbit Antibody. Sigma Aldrich St Louis, MO. C6219
Muscarinic Acetylcholine Receptor Type 2	1:1000	Monoclonal Mouse Antibody. Novus Biologicals, Littleton CO. 31-1D1
Beta-Adrenergic Receptor Type 1	1:1000	Polyclonal Rabbit Antibody. Abcam. San Francisco, CA. ab103653

<b>Secondary Antibody</b>	<b>Concentration</b>	<b>Source</b>
Cy3 AffiniPure Donkey Anti-Rabbit IgG	1:400	Polyclonal Rabbit Antibody. Jackson ImmunoResearch Laboratories, Inc. West Grove PA. 711-165-152.
Alexa Flour 488 AffiniPure Donkey Anti-Sheep IgG	1:400	Polyclonal Sheep Antibody. Jackson ImmunoResearch Laboratories, Inc. West Grove PA. 713-545-003.
Alexa Flour 647 AffiniPure Donkey Anti-Mouse IgG	1;400	Polyclonal Mouse Antibody. Jackson ImmunoResearch Laboratories, Inc. West Grove PA. 715-605-150.

## **RNA Sequencing**

Following termination, hearts were rapidly excised, and border zone samples marked prior to termination were collected, rinsed in chilled saline, and snap frozen in liquid nitrogen. RNA was isolated using QIAGEN RNeasy column (Qiagen Sciences, Germantown, MD). Total RNA quality was checked on an Agilent Bioanalyzer 2100 system (Agilent Technologies Inc, Santa Clara, CA), while RNA concentration was measured with Nanodrop spectrophotometer (ThermoFisher Scientific, Canoga Park, CA). Libraries were prepared for RNA sequencing with KAPA Stranded RNA-Seq Kit (Roche Sequencing Solutions, Pleasanton, CA). The workflow consisted of mRNA enrichment, cDNA generation, and end repair to generate blunt ends, A-tailing, adaptor ligation, and PCR amplification. Different adapters were used for multiplexing samples in one lane. Sequencing was performed on Illumina HiSeq3000 for a single read 50 run. Data quality check was done on Illumina SAV. Demultiplexing was performed with Illumina Bcl2fastq2 v 2.17 program.

The reads were mapped to the latest UCSC transcript set using Bowtie2 version 2.1.0(36) and the gene expression level was estimated using RSEM v1.2.15(37). edgeR(38) was used to calculate differential expression. Count normalization was performed with edgeR's TMM algorithm. Genes that had a fold change (FC)  $\geq 1.5$  and pvalue  $\leq 0.05$  were called a differentially expressed. Upon manuscript acceptance, RNA-seq data will be deposited in Geo and made freely available.

## RT PCR

Immediately after transmural biopsy of left ventricular scar-border zone myocardium, tissues were snap frozen in liquid nitrogen and stored at -80 °C. Tissues were homogenized with Trizol (Thermo Fisher Scientific Inc., USA). Chloroform (200µL for each 1mL TRIZOL) was added, incubated for 3 minutes and then centrifuged(12000g for 15minutes). RNA was extracted and incubated at 25°C for 10 minutes using a Random Hexamer Primer (Thermo Fisher scientific Inc., USA). cDNA was purified after reverse transcription (48°C for 30 minutes) followed by inactivation of reverse transcription at 95°C for 5 minutes. Real-time PCR was performed for ion channel analysis using an Applied Biosystems 7900HT sequence detector or Applied Biosystems Quant Studio 6 Flex per manufacturer's directions.

List of primers used.

	Forward	Reverse
SCN5A	CATGCGGGTTGTGGTCAATG	CGCAGTCGCTCTTGTTGTTTC
HERG/KCNH2	TGGACACCATCATCCGCAAG	AAGCAGCTCCCATCTTTCCG
KCNQ1	AGGTCATTCGACGTATGCAGT	GTCCAGCTGTGTCACCTTGTC
Ito/KCND2	AACGGAGAGCACAAAAGAAAGC	CTGAGTAGGCCGTTCCGTTT
Ik1/KCNJ4	ATAAACTTGGCCCTGCGTCTT	AGGTTGGCGAAGTACACGTT
SERCA/ATPA2	TACCCAATGACAATGGCGCT	CCATCGGTACATGCCGAGAA
SERCA/ATPA3	TCTTTGAGTCACGCTTCCCC	CCTTTTCTTCGTCCACGTGCT
RyR2	GCTGGCCTCTACAACCACTT	ACAGGACATCCAGCACCTTG
CaV1.2/CACNA1c	ATCCCTTTCCGGAGGATGA	ACTGAAAAGCCCGACAACCA
ADRB1	GCGATTCGTCACCAACAGG	ATGCACAAGGGCACGTAGAA
CHRM2	ACTCATCTTCCTTATGAAGGCCA	ATACACATTTAAACCTGCCGC
GAPDH	AGTGAACGGATTTGGCCGC	TTCATGGTTCACGCCCATC
Actin	GATCAAGATCATCGCGCCTC	CTGCAGGTCCCGAGAGAATG
Cyclophilin	GAGCTGTTTGCAGACAAAGTT	GTTTGCCATCCAACCACTCA

## Statistical Analysis

Variables are presented as means  $\pm$  standard error (SE). The Shapiro-wilk test was used for assessing distribution. A student t-test and ANOVA test were used for data that were normally distributed, and the Mann-Whitney test and Kruskal-Wallis test were used for data that were not normally distributed. \*Indicated statistical significance at  $p$  value  $< 0.05$  (\*\*denotes  $p$  value  $< 0.01$ , \*\*\*denotes  $p$  value  $< 0.001$ , \*\*\*\*denotes  $p$  value  $< 0.0001$ ). Analysis was performed using Graphpad Prism (La Jolla, CA, USA).

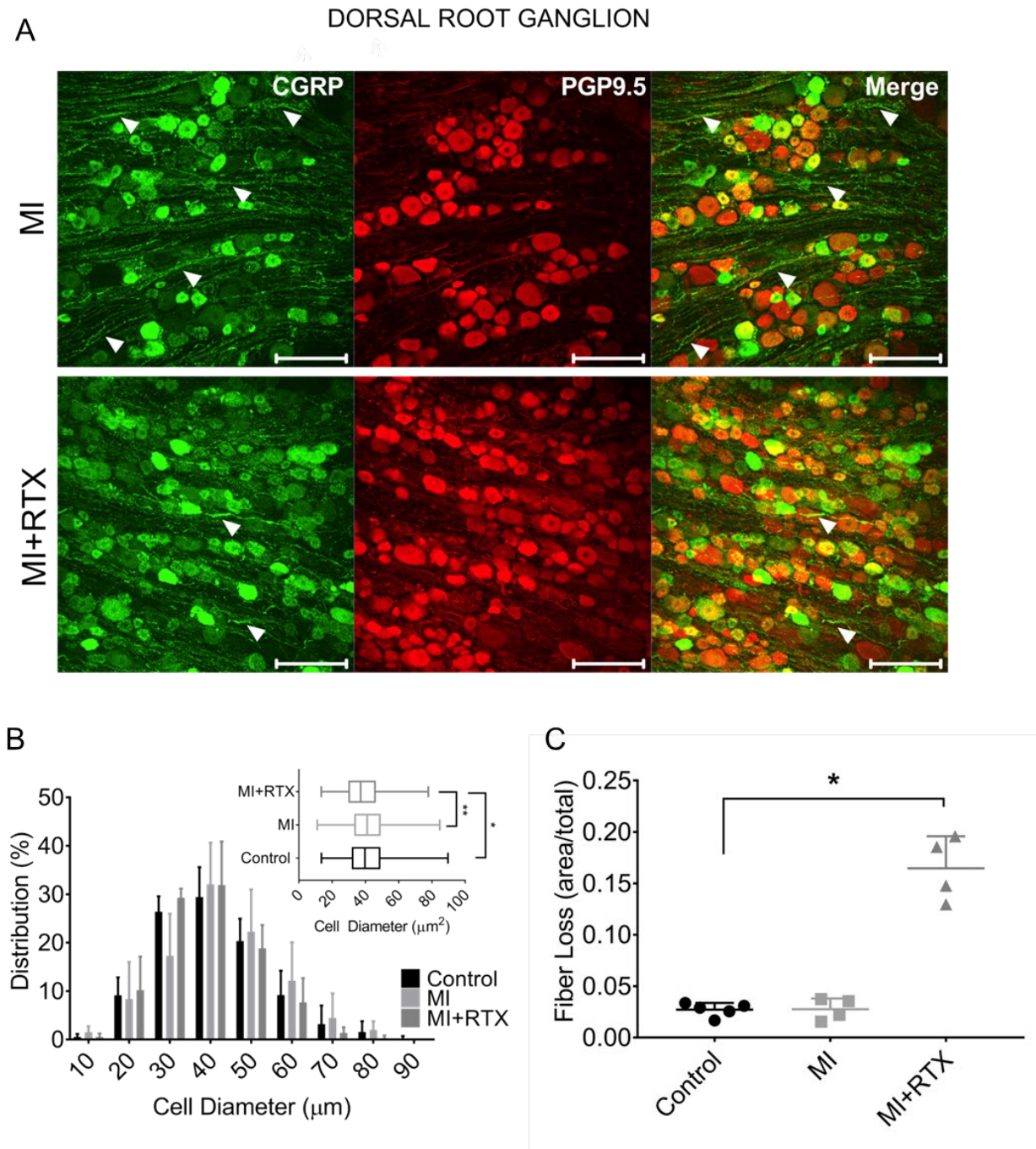
## REFERENCES

1. Beaumont E, Salavatian S, Southerland EM et al. Network interactions within the canine intrinsic cardiac nervous system: implications for reflex control of regional cardiac function. *The Journal of physiology* 2013;591:4515-33.
2. Rajendran PS, Nakamura K, Ajjola OA et al. Myocardial infarction induces structural and functional remodelling of the intrinsic cardiac nervous system. *The Journal of physiology* 2016;594:321-41.
3. Ardell JL, Andresen MC, Armour JA et al. Translational Neurocardiology: preclinical models and cardioneural integrative aspects. *The Journal of physiology* 2016.
4. Shivkumar K, Ajjola OA, Anand I et al. Clinical neurocardiology-defining the value of neuroscience-based cardiovascular therapeutics. *The Journal of physiology* 2016.
5. O'Gara PT, Kushner FG, Ascheim DD et al. 2013 ACCF/AHA guideline for the management of ST-elevation myocardial infarction: executive summary: a report of the American College of Cardiology Foundation/American Heart Association Task Force on Practice Guidelines: developed in collaboration with the American College of Emergency Physicians and Society for Cardiovascular Angiography and Interventions. *Catheterization and cardiovascular interventions : official journal of the Society for Cardiac Angiography & Interventions* 2013;82:E1-27.
6. Brown AM. Excitation of afferent cardiac sympathetic nerve fibres during myocardial ischaemia. *The Journal of physiology* 1967;190:35-53.
7. Malliani A, Schwartz PJ, Zanchetti A. A sympathetic reflex elicited by experimental coronary occlusion. *The American journal of physiology* 1969;217:703-9.
8. Malliani A, Recordati G, Schwartz PJ. Nervous activity of afferent cardiac sympathetic fibres with atrial and ventricular endings. *The Journal of physiology* 1973;229:457-69.
9. Wang W, Schultz HD, Ma R. Cardiac sympathetic afferent sensitivity is enhanced in heart failure. *Am J Physiol* 1999;277:H812-7.

10. Zahner MR, Li DP, Chen SR, Pan HL. Cardiac vanilloid receptor 1-expressing afferent nerves and their role in the cardiogenic sympathetic reflex in rats. *J Physiol* 2003;551:515-23.
11. Caterina MJ, Schumacher MA, Tominaga M, Rosen TA, Levine JD, Julius D. The capsaicin receptor: a heat-activated ion channel in the pain pathway. *Nature* 1997;389:816-24.
12. Karai L, Brown DC, Mannes AJ et al. Deletion of vanilloid receptor 1-expressing primary afferent neurons for pain control. *The Journal of clinical investigation* 2004;113:1344-52.
13. Wang HJ, Wang W, Cornish KG, Rozanski GJ, Zucker IH. Cardiac sympathetic afferent denervation attenuates cardiac remodeling and improves cardiovascular dysfunction in rats with heart failure. *Hypertension* 2014;64:745-55.
14. Yoshie K, Rajendran PS, Massoud L et al. Cardiac vanilloid receptor-1 afferent depletion enhances stellate ganglion neuronal activity and efferent sympathetic response to cardiac stress. *American journal of physiology Heart and circulatory physiology* 2018;314:H954-H966.
15. Price TJ, Flores CM. Critical evaluation of the colocalization between calcitonin gene-related peptide, substance P, transient receptor potential vanilloid subfamily type 1 immunoreactivities, and isolectin B4 binding in primary afferent neurons of the rat and mouse. *The journal of pain : official journal of the American Pain Society* 2007;8:263-72.
16. Lawson SN, Perry MJ, Prabhakar E, McCarthy PW. Primary sensory neurones: neurofilament, neuropeptides, and conduction velocity. *Brain research bulletin* 1993;30:239-43.
17. Marban E, Robinson SW, Wier WG. Mechanisms of arrhythmogenic delayed and early afterdepolarizations in ferret ventricular muscle. *J Clin Invest* 1986;78:1185-1192.
18. Pinto JM, Boyden PA. Electrical remodeling in ischemia and infarction. *Cardiovascular research* 1999;42:284-97.
19. Dillon SM, Allessie MA, Ursell PC, Wit AL. Influences of anisotropic tissue structure on reentrant circuits in the epicardial border zone of subacute canine infarcts. *Circulation research* 1988;63:182-206.
20. Landstrom AP, Dobrev D, Wehrens XHT. Calcium Signaling and Cardiac Arrhythmias. *Circulation research* 2017;120:1969-1993.
21. Ajjola OA, Lux RL, Khaheera A et al. Sympathetic modulation of electrical activation in normal and infarcted myocardium: implications for arrhythmogenesis. *American journal of physiology Heart and circulatory physiology* 2017;312:H608-H621.
22. Peters NS, Coromilas J, Severs NJ, Wit AL. Disturbed connexin43 gap junction distribution correlates with the location of reentrant circuits in the epicardial border zone of healing canine infarcts that cause ventricular tachycardia. *Circulation* 1997;95:988-996.
23. Ziegler KA, Ahles A, Wille T, Kerler J, Ramanujam D, Engelhardt S. Local sympathetic denervation attenuates myocardial inflammation and improves cardiac function after myocardial infarction in mice. *Cardiovascular research* 2017;114:291-299.
24. Perlini S, Palladini G, Ferrero I et al. Sympathectomy or doxazosin, but not propranolol, blunt myocardial interstitial fibrosis in pressure-overload hypertrophy. *Hypertension* 2005;46:1213-8.

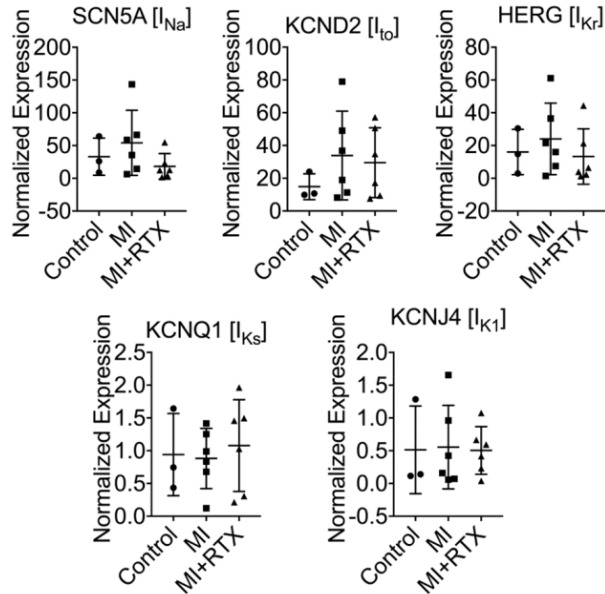
25. Zhong B, Rubinstein J, Ma S, Wang DH. Genetic ablation of TRPV1 exacerbates pressure overload-induced cardiac hypertrophy. *Biomedicine & pharmacotherapy = Biomedecine & pharmacotherapie* 2018;99:261-270.
26. Huang W, Rubinstein J, Prieto AR, Thang LV, Wang DH. Transient receptor potential vanilloid gene deletion exacerbates inflammation and atypical cardiac remodeling after myocardial infarction. *Hypertension* 2009;53:243-50.
27. Andrei SR, Sinharoy P, Bratz IN, Damron DS. TRPA1 is functionally co-expressed with TRPV1 in cardiac muscle: Co-localization at z-discs, costameres and intercalated discs. *Channels (Austin, Tex)* 2016;10:395-409.
28. Hurt CM, Lu Y, Stary CM et al. Transient Receptor Potential Vanilloid 1 Regulates Mitochondrial Membrane Potential and Myocardial Reperfusion Injury. *Journal of the American Heart Association* 2016;5.
29. Skinner JE, Lie JT, Entman ML. Modification of ventricular fibrillation latency following coronary artery occlusion in the conscious pig. *Circulation* 1975;51:656-67.
30. Workman AJ, Kane KA, Rankin AC. The contribution of ionic currents to changes in refractoriness of human atrial myocytes associated with chronic atrial fibrillation. *Cardiovascular research* 2001;52:226-35.
31. Reuter H, Han T, Motter C, Philipson KD, Goldhaber JJ. Mice overexpressing the cardiac sodium-calcium exchanger: defects in excitation-contraction coupling. *The Journal of physiology* 2004;554:779-89.
32. Ajjola OA, Lux RL, Khahera A et al. Sympathetic Modulation of Electrical Activation In Normal and Infarcted Myocardium: Implications for Arrhythmogenesis. *Am J Physiol Heart Circ Physiol* 2017:ajpheart 00575 2016.
33. Ajjola OA, Yagishita D, Patel KJ et al. Focal myocardial infarction induces global remodeling of cardiac sympathetic innervation: neural remodeling in a spatial context. *American journal of physiology Heart and circulatory physiology* 2013;305:H1031-40.
34. Millar CK, Kralios FA, Lux RL. Correlation between refractory periods and activation-recovery intervals from electrograms: effects of rate and adrenergic interventions. *Circulation* 1985;72:1372-9.
35. Lewicki MS. A review of methods for spike sorting: the detection and classification of neural action potentials. *Network (Bristol, England)* 1998;9:R53-78.
36. Langmead B, Salzberg SL. Fast gapped-read alignment with Bowtie 2. *Nature methods* 2012;9:357-9.
37. Li B, Dewey CN. RSEM: accurate transcript quantification from RNA-Seq data with or without a reference genome. *BMC bioinformatics* 2011;12:323.
38. Robinson MD, McCarthy DJ, Smyth GK. edgeR: a Bioconductor package for differential expression analysis of digital gene expression data. *Bioinformatics (Oxford, England)* 2010;26:139-40.

## SUPPLEMENTAL FIGURES

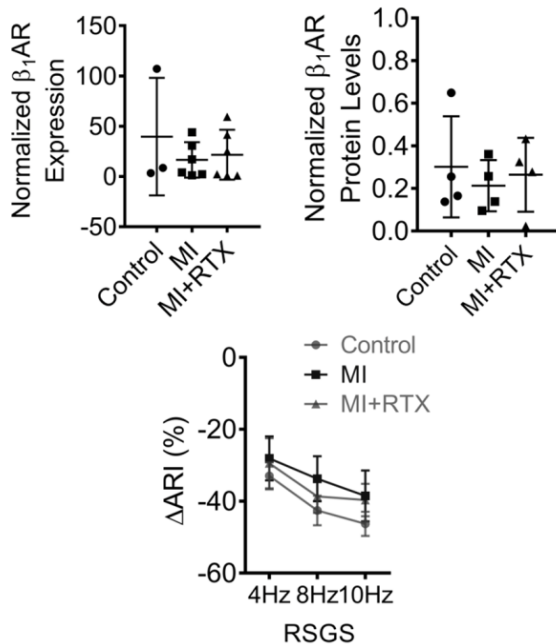


**Supplemental Figure 1. Chemical depletion of cardiac TRPV1 afferents by resiniferatoxin.** (A) Representative images of DRGs from MI and MI+RTX subjects, showing regions of fiber loss seen in MI+RTX but not in MI. Arrowheads shown regions of preserved fiber bundles are reduced in MI+RTX subjects. (B) DRG cell size distribution shows that epicardial RTX administration did not deplete soma, as there no upshift in cell size. Rather, mean soma size was reduced in MI+RTX compared to control and MI subjects. (C) Quantification of regions showing fiber loss across serial sections of DRGs from each group, as shown in panel (A). These data suggest that RTX caused chemoaxotomy of cardiac sympathetic afferents expressing TRPV1 (n=497, 300, and 511 for Control, MI, and MI+RTX, respectively). \*p<0.05, \*\* p<0.01. (B) ANOVA, and (C) Kruskal-Wallis tests.

A



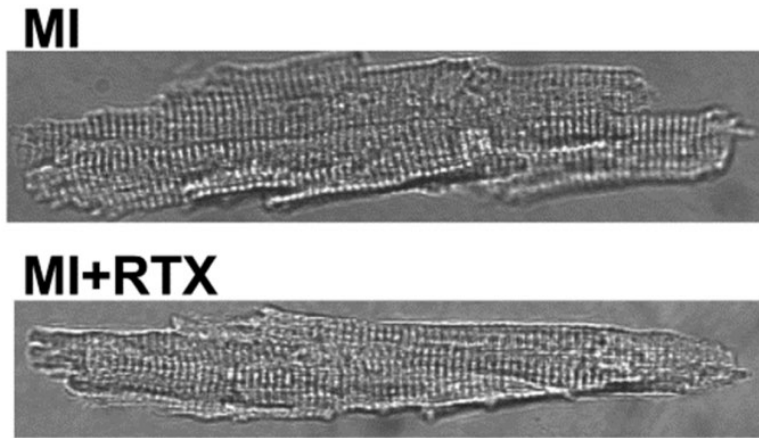
B



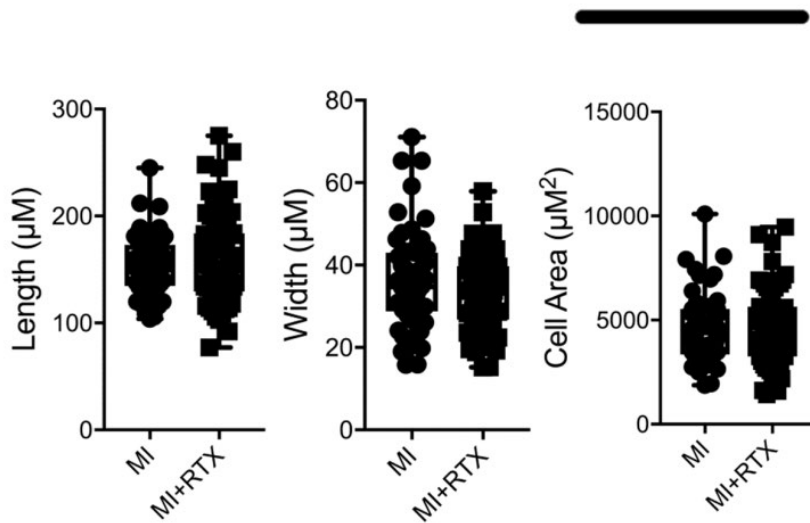
### Supplemental Figure 2. Ion channel and Beta-1 Adrenergic receptor expression.

**(A)** Normalized fold expression of the key ion channels that constitute myocardial action potential from quantitative reverse transcriptase polymerase chain reaction (qRT-PCR) reveals no significant differences between control, myocardial infarction (MI), and resiniferatoxin (RTX)-treated MI subjects (MI+RTX). **(B)** Similarly,  $\beta_1$ -adrenergic receptor expression, relative protein levels quantified by Western blotting, and change in activation recovery interval (ARI, a surrogate for action potential duration) to stepwise increase in right stellate ganglion stimulation (RSGS) were not different between the groups.

A

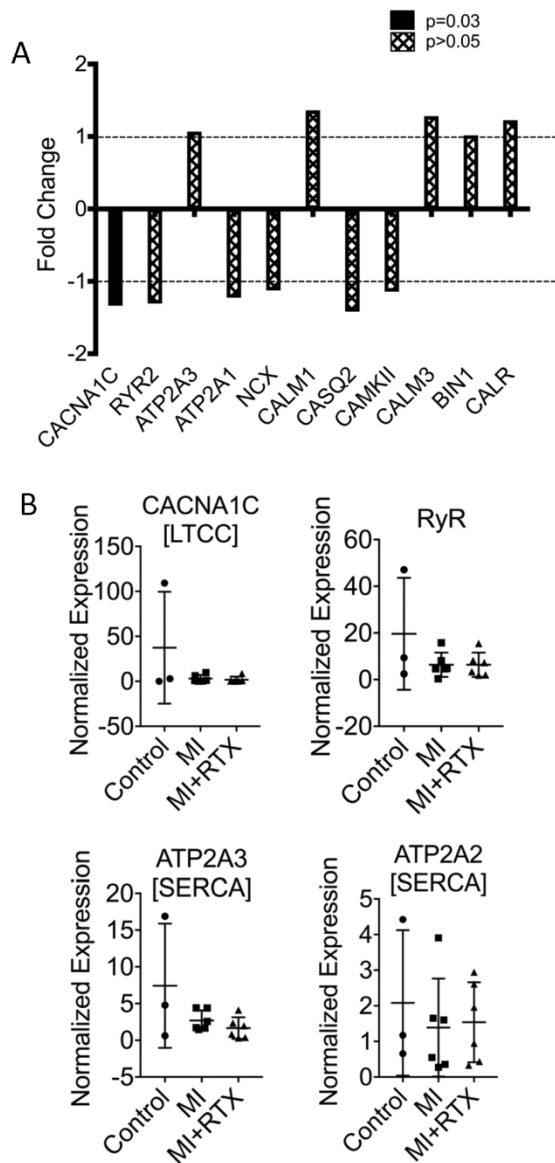


B

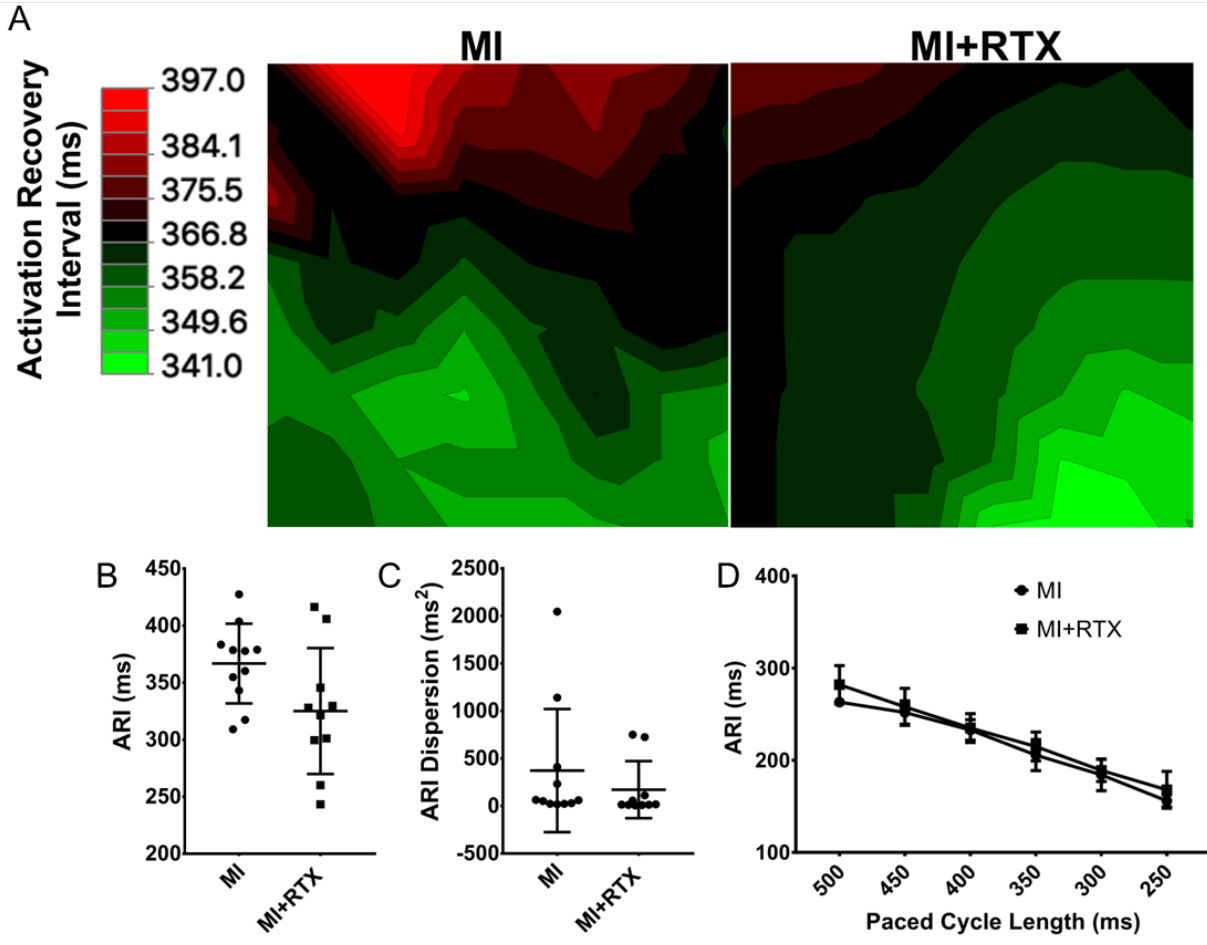


**Supplemental Figure 3. Isolated scar-border zone cardiomyocytes are not morphologically different after RTX treatment.**

**(A)** Representative images and **(B)** quantified data showing no differences between MI and MI+RTX cells in length, width, and area. Scale bar: 50 $\mu\text{M}$ .

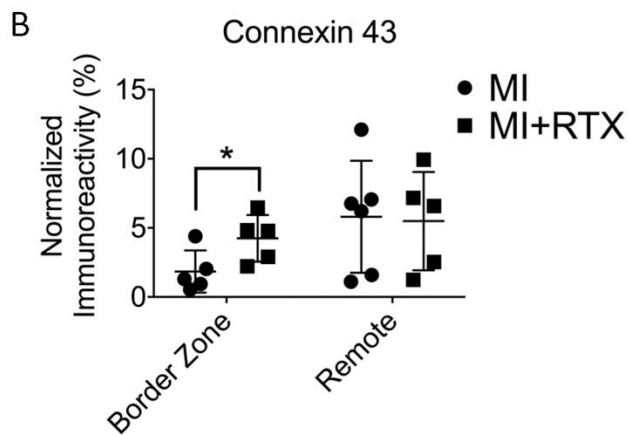
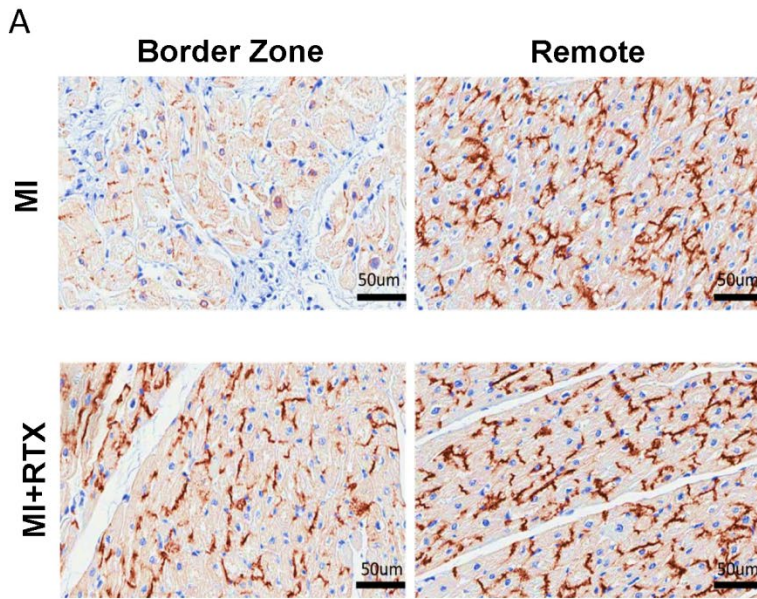


**Supplemental Figure 4. Expression of channels and proteins involved in calcium regulation.** (A) Bar graph showing fold expression from RNA sequencing (RNA-seq) of the key channels and handling proteins involved in cardiomyocyte calcium regulation. (B) Quantitative RT-PCR validation of some of the RNA-seq results showing no differences in the expression calcium handling proteins and channels.



**Supplemental Figure 5. Cardiac TRPV1 afferent depletion does not alter scar-border zone repolarization properties.**

(A) Representative sinus rhythm activation recovery interval maps (ARI, a surrogate for action potential duration) measured from scar-border zone epicardial electrograms. There were no differences in (B) mean ARI, (C) ARI dispersion (variance), and (D) ARI restitution using the standard dynamic (rapid pacing) method.

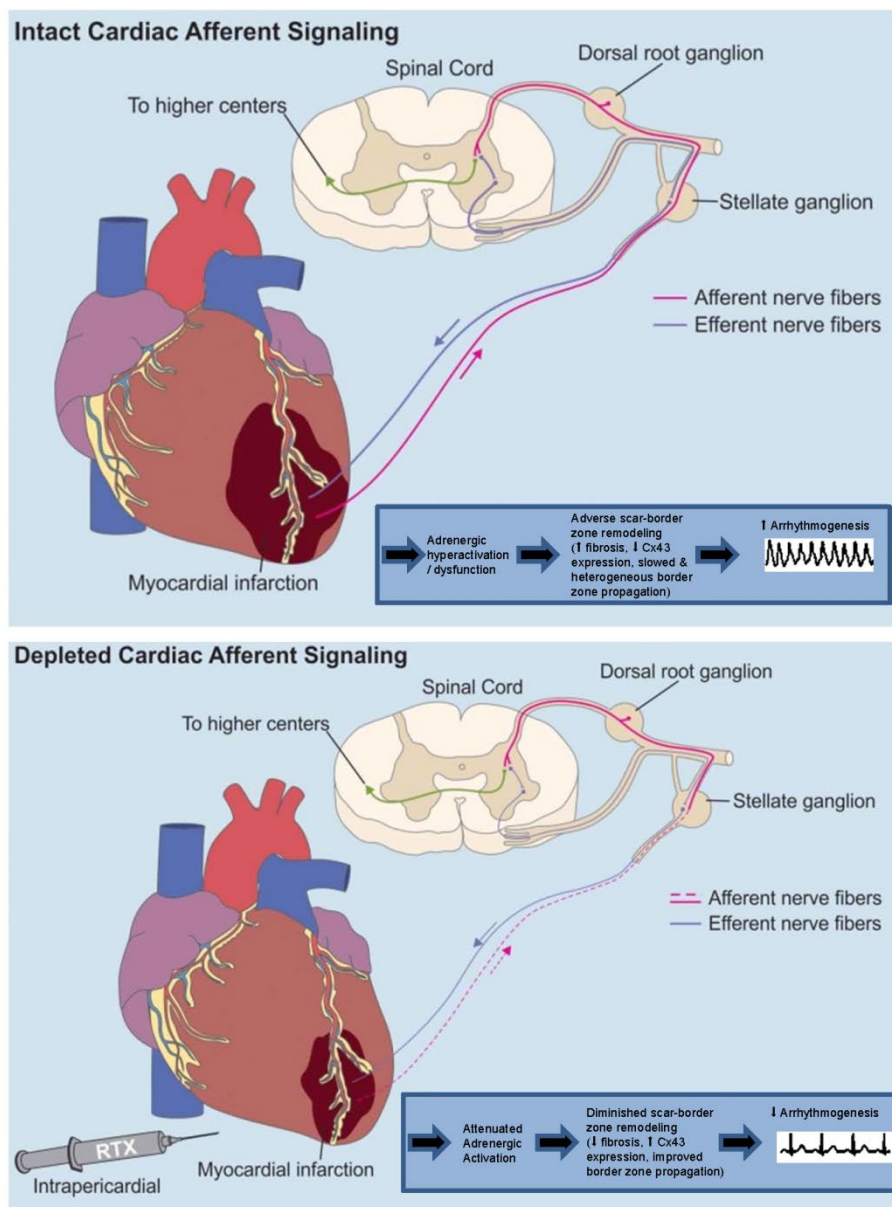


**Supplemental Figure 6. Connexin 43 remodeling in scar-border zones is reduced by cardiac afferent chemo-axotomy.**

(A) Representative images from border zone and remote myocardium of myocardial infarct (MI) and resinfiferatoxin-treated MI subjects (MI+RTX) showing reduced immunoreactivity for connexin 43.

(B) Quantified data across subjects (n=5/group). \*p=0.023.

## Graphical Abstract



**Supplemental Figure 7. Mechanisms mediating the antiarrhythmic effects of cardiac TRPV1 afferent chemo-axotomy after myocardial infarction.**